ACS APPLIED MATERIALS & INTERFACES

www.acsami.org

Research Article

Irregular Wind Energy Harvesting by a Turbine Vent Triboelectric Nanogenerator and Its Application in a Self-Powered On-Site Industrial Monitoring System

Jianjun Zhang, Yanshuo Sun, Jin Yang, Tao Jiang, Wei Tang, Baodong Chen,* and Zhong Lin Wang*

Cite This: https://doi.org/10.1021/acsami.1c16680

Read Online

ACCESS | Metrics & More | Article Recommendations | Supporting Information

ABSTRACT: Wind is a regenerative and sustainable green energy, but it is intermittent; especially, harvesting irregular wind energy is a great challenge for existing technologies. This study demonstrates a turbine vent triboelectric nanogenerator (TV-TENG), which can be utilized as both an irregular wind harvester and a self-powered environmental sensing system on the rooftops of buildings. At a wind speed of nearly 7 m/s, the TV-TENG delivers an open-circuit voltage of up to 178.2 V, a short-circuit current of 38.2 μA, and a corresponding peak power of 2.71 mW under an external load of 5 MΩ, which can be used to directly light up 120 green light-emitting diodes. Furthermore, a self-powered on-site industrial monitoring system has been developed, which can be improve the easiness and simpleness of the industry environment for temperature monitoring and safety warning. Increasing the fluidity of air inside and outside the device is a key factor in fabricating an efficient TV-TENG; it is a novel approach for harvesting irregular wind energy and is sensitive, reliable, waterproof, and easy to use. This work greatly expands the applicability of TENGs as energy harvesters for irregular wind and also as self-powered sensing systems for ambient detection.

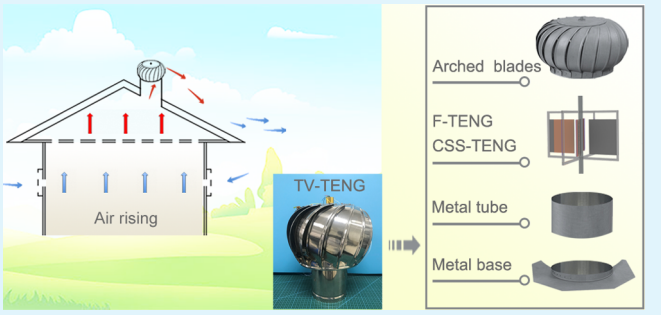

KEYWORDS: *triboelectric nanogenerator, turbine vent, irregular wind energy, self-powered system, distributed energy*

Downloaded via GEORGIA INST OF TECHNOLOGY on November 16, 2021 at 15:04:25 (UTC).
See https://pubs.acs.org/sharingguidelines for options on how to legitimately share published articles.

1. INTRODUCTION

In recent years, micro−nano mechanical energy harvesting from the environment and converting it into electricity have attracted a great deal of research interest.[1,2] Wind energy is a widespread inexhaustible supply by nature and is regenerative and clean, so it is likely to be a part of the solution to the atmospheric carbon dioxide and the global warming problem.[3−9] In fact, the conventional wind power generation technologies rely on turbines and the principle of electromagnetic induction.[10,11] However, the aforementioned conventional techniques are still unable to cope with in complex working environments,[1] such as irregular winds,[12] upper-air winds,[13,14] random and weak winds in our daily living environment, and so forth. Therefore, researchers throughout the world are working on developing a matched power technology for harvesting irregular and wasteful wind energy, which is significant to tackling climate change by reducing its carbon footprint and moving towards carbon neutrality.[15,16]

In this regard, it is essential to develop innovative strategies in the energy technologies to collect irregular wind energy from the environment. Since the invention of the triboelectric nanogenerator (TENG, called Wang's generator) in 2012 by Z. L. Wang's research group,[17] it was extensively investigated and has shown lots of advantages including simple design, high power density, high sensitivity, and rapid response.[18,19] As a great potential micro−nano energy technology, the TENG was proposed to solve these issues, which has proved to be an effective method to convert micro−nano mechanical energy into electricity or electrical signals by the coupling effect between triboelectrification and electrostatic induction,[20,21] such as vibration,[22−25] sliding,[26] and rotation[27−29] in a living environment. So far, a variety of TENG devices have been designed to harvest wind energy,[30−32] demonstrating the huge potential for the efficient use of wind energy to generate electricity. Moreover, TENGs have been utilized as self-powered sensors for monitoring wind speed,[33,34] vibration,[35] and displacement.[36,37] However, the utilization efficiency of irregular wind energy is unbelievably low in the current technologies,[38] and it is difficult for normal working due to the low operating frequency of most devices when the speed of wind is less than 3 m/s.[39,40] Thus, the constantly developing TENGs are of great importance to harvest irregular wind

Received: September 6, 2021
Accepted: October 28, 2021

© XXXX American Chemical Society

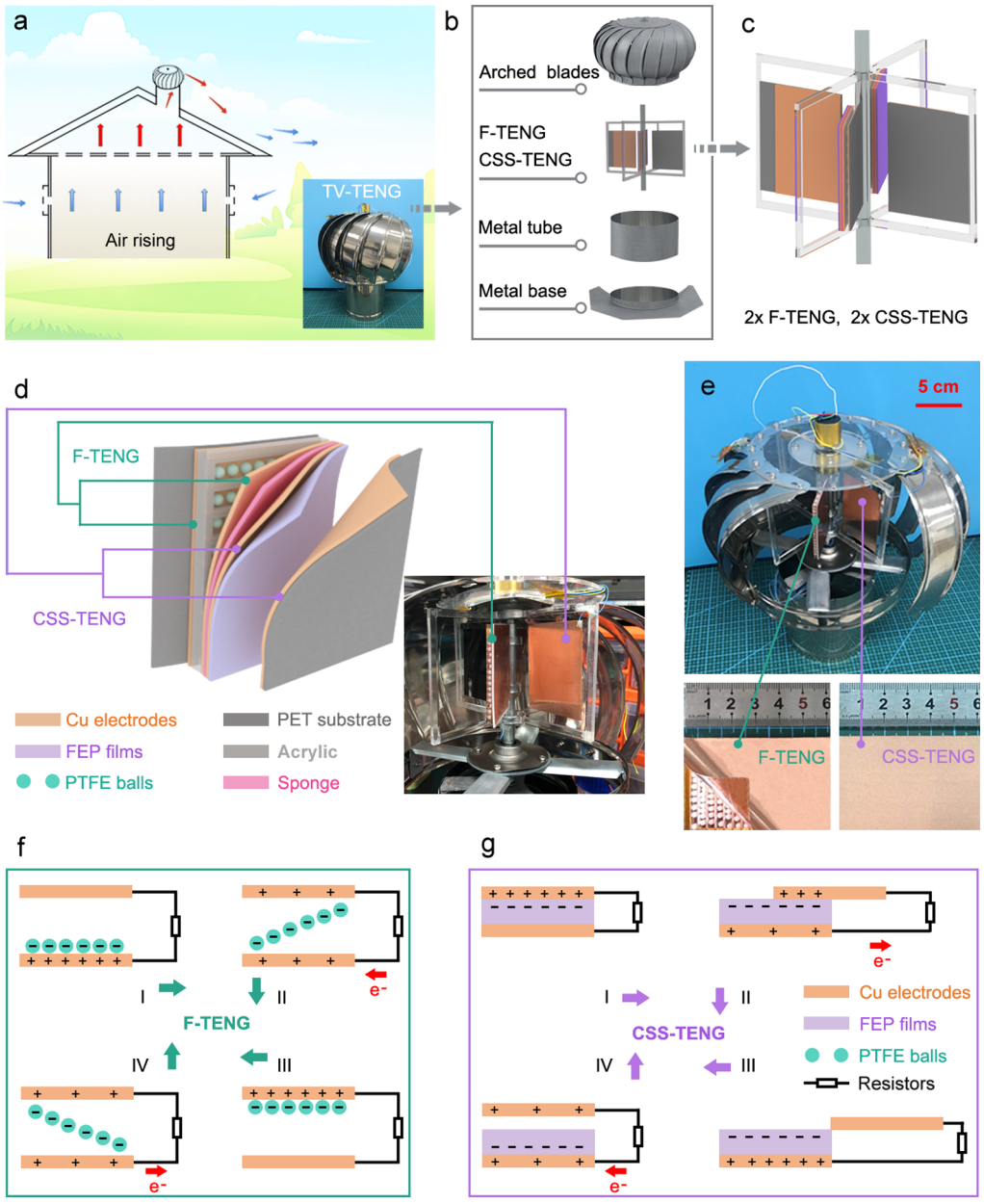

Figure 1. Schematic structure and electricity generation principles of the TV-TENG. (a) Schematic diagram showing the application scenario of the TV-TENG. (b) Detailed exploded views of the TV-TENG. (c) Core structure of the TV-TENG by integrating the two F-TENG units and two CSS-TENG units. (d) Detailed structure of one electricity generation unit and its photographs. (e) Photographs of the whole TV-TENG device and its inside structure. (f,g) Working principles of the F-TENG and CSS-TENG in a full cycle under the wind-induced vibration energy.

energy, which not only decrease the cost and reduce the waste of irregular wind energy but also greatly expand the applications of TENGs.

In this article, we report a turbine vent TENG (TV-TENG) that converts irregular wind directly into electrical energy, which is a sustainable power source to achieve real-time monitoring and safety warning for the self-powered sensing system. Because the turbine vent has a good waterproof function, the TV-TENG can work in harsh environments whether the weather is sunny or rainy. The TV-TENG is composed of two freestanding mode TENGs (F-TENGs) and two contact-sliding-separation mode TENGs (CSS-TENGs) and integrated together on a turbine vent with a volume of about 0.0064 m^3. It was designed to efficiently achieve sliding/vibration energy harvesting caused by the irregular wind between adjacent buildings. The F-TENG can collect mechanical energy more effectively because it would vibrate many times after one trigger. The TV-TENG unit generates an open-circuit voltage of up to 178.2 V, a short-circuit current of 38.2 μA, and a corresponding peak power of 2.71 mW under an external load of 5 MΩ, which can be used to directly light up 120 green light-emitting diodes (LEDs). Furthermore, self-powered temperature sensing and wireless early warning systems have been successfully developed, respectively.

2. RESULTS AND DISCUSSION

2.1. Structure of the TV-TENG. The fabricated TV-TENG consists of two F-TENGs and two CSS-TENGs and a turbine vent with a volume of about 0.0064 m^3 (it is made up of some arched blades, one central axle, two bearings, a fixing

https://doi.org/10.1021/acsami.1c16680
ACS Appl. Mater. Interfaces XXXX, XXX, XXX−XXX

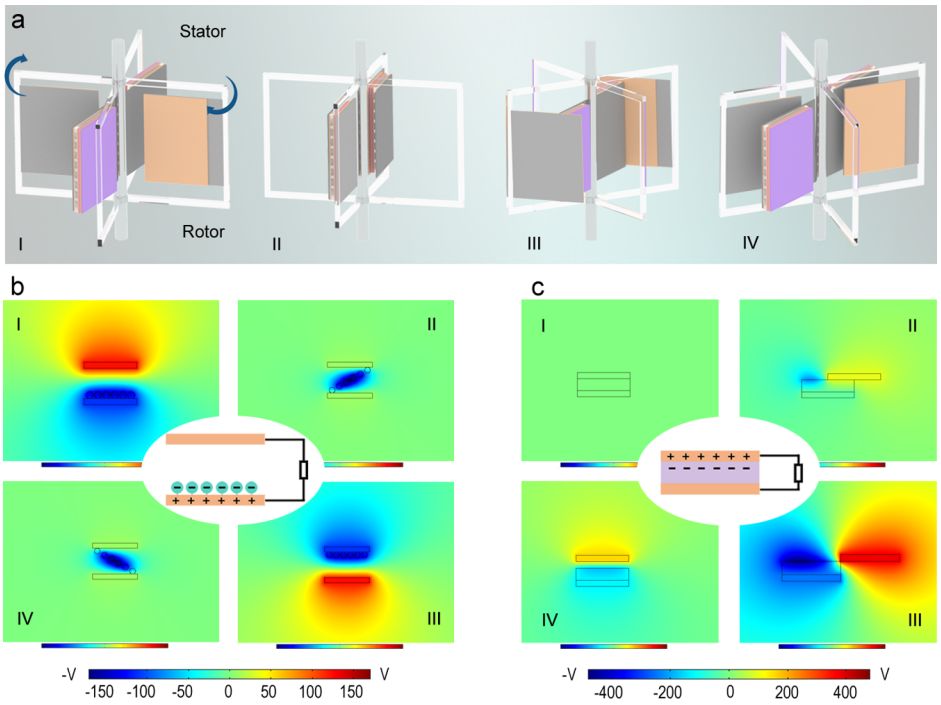

Figure 2. Working process and electrical potentials distribution of the TV-TENG. (a) Diagrammatic drawing showing the working process of the TV-TENG consisting of the F-TENG and CSS-TENG. (b,c) Numerically calculated electrical potentials distribution of the F-TENG and CSS-TENG.

bracket, a metal tube, and a base), as schematically illustrated in Figure 1. The application scenario of the TV-TENG and the detailed expanded views of the structure is schematically illustrated in Figure 1a−c. The TV-TENG is composed of one turbine vent and two sets of F-TENGs and two sets of CSS-TENGs. The outside of the TV-TENG is the turbine vent shell made of 304 stainless steel and the inside contains two types of TENGs, as shown in Figure 1c. When the wind on the roof drives the TV to rotate, it can not only exhaust the hot or dirty air in the room but also drive the TENG to work to generate electricity. The key electricity generation unit of the TV-TENG is composed of a stator and a rotor on the fixing bracket. The stator consists of three copper (Cu) foils (i, ii, and iii), some small polytetrafluoroethylene (PTFE) balls (a diameter of 2.15 mm), an acrylic gridded frame, a fluorinated ethylene propylene (FEP) film, a sponge, and a polyethylene terephthalate (PET) substrate and is used to form an F-TENG unit with a size of 4 × 6 cm. The rotor consists of Cu foil (iv), a PET substrate membrane, and a rectangular acrylic framework and is used to form a CSS-TENG unit with the same size of 4 × 6 cm. One side of Cu foil (iv) and PET membrane is fixed on the sidewall of the framework, leaving the other side free-standing. Cu foil (iv) plays dual roles as a triboelectric surface and as an electrode, as shown in Figure 1d. The photograph of the internal structure is illustrated in Figure 1e. More details on the preparation of the TV-TENG are given in Supporting Information.

The output of the F-TENG is based on periodic contact−separation between two Cu foils (i and ii) and some PTFE balls which from an ongoing vibration caused by the spinning of TV-TENG. On the other hand, the distance between Cu foil (iv) and FEP film/backing Cu foil (iii) can be changed periodically due to the irregular wind-induced rotation of the CSS-TENG, leading to contact−sliding−separation and resulting in an electrical output across an external loading resistor. Furthermore, the TV-TENG can ensure that it is protected from rain under harsh working conditions and effectively use irregular wind energy in any parallel direction, which is attributed to the optimized structure design of the arched blades of the turbine vent.

2.2. Working Principle of the TV-TENG. A full cycle of the electricity generation processes of the integrated TV-TENG is presented in Figure 1f,g in which the basic unit consists of an F-TENG unit and a CSS-TENG unit. The coupled effect between triboelectrification and electrostatic induction produces an alternating charge flow in external load to form a sustainable power source. The working principle of the F-TENG unit is basically in accordance with the freestanding mode.[41] When the device is placed in an irregular wind environment, the PTFE balls in the acrylic frame directly collide up and down between the two Cu foils (i and ii) as driven by irregular wind vibration (Figure 1f). In the first step (I), it would form negative charges on the surface of the PTFE balls when the PTFE balls come into contact with Cu foil (i) at the bottom of the acrylic frame and form positive charges on the surface of Cu foil (i) due to the material triboelectric series.[42] In the second step (II), the negative charges will flow from Cu foil (ii) to Cu foil (i) to achieve a new electrostatic balance when the PTFE balls move upward, forming a current under the short-circuit condition. In the third step (III), after the PTFE balls collide with the Cu foil (ii) and will be about to move downward, the negative charges in Cu foil (ii) will flow to Cu foil (i) to return to the original electrostatic status. In the fourth step (IV), contrary to the second step II, it would form a reverse current under the short-circuit condition when the PTFE balls move downward and will restore to the original state (Step I). These four steps form the fundamental working processes of converting irregular wind vibration energy into electricity. The working principle of the CSS-TENG is based on the sliding and contact−separation mode, in which the

https://doi.org/10.1021/acsami.1c16680
ACS Appl. Mater. Interfaces XXXX, XXX, XXX−XXX

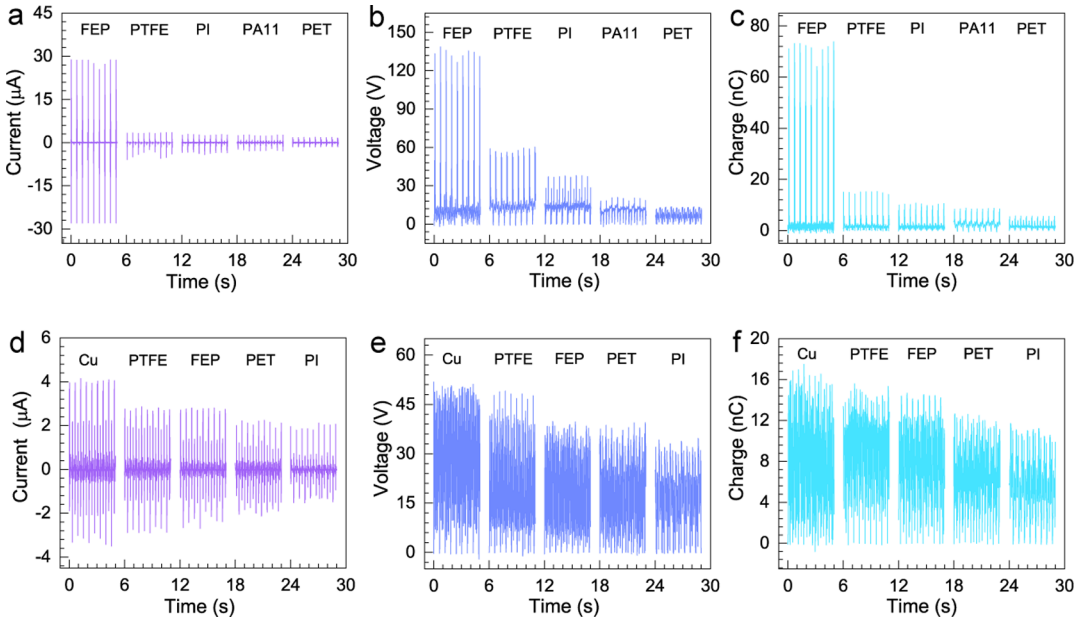

Figure 3. Electrical output performances of the F-TENG and CSS-TENG with different triboelectric materials. (a,d) Short-circuit current of the F-TENG and CSS-TENG. (b,e) Open-circuit voltage of the F-TENG and CSS-TENG. (c,f) Ttransferred charge of the F-TENG and CSS-TENG.

triboelectric FEP film/backing Cu foil (iii) on the outer layer of the F-TENG is shared. It includes four typical steps, as shown in Figure 1g. At the initial step (I), the FEP film/backing Cu foil (iii) and Cu foil (iv) on the rotor are in a contact state without current flow or electrical potentials, in which Cu foil (iv) plays dual roles as a triboelectric surface and an electrode. When the two contact surfaces are in the state of relative sliding (step II) and reach a separated state (step III), the resulting charge separation will induce a positive potential on Cu foil (iii) and the positive charges will be driven from Cu foil (iv) to Cu foil (iii). Sequentially, going through step (III) and step (IV) to step (I), that is Cu foil (iv) approaches Cu foil (iii) and re-contacts in the working process, forms the exact reverse current in the external circuit. Finally, contacting and separating of Cu foil (iv) from the FEP film would change the local electrostatic field, so that positive charges exchange between the two Cu foils to maintain the potential change. In summary, the electricity generation principles of the TV-TENG generated triboelectric potential difference based on the contact/separation between two triboelectric materials to drive the electrostatic induction charge flow in the external circuit.

To obtain a more quantitative understanding and theoretical prediction of the proposed electricity generation principles of the TV-TENG, the electric potential distribution and the charge transfer can be verified through finite-element simulation using COMSOL software.[43,44] Figure 2a illustrates a working process of the TV-TENG, including two F-TENGs (the stator in the diagram, 40 × 60 mm) and two CSS-TENGs (the rotor in the diagram, 4 × 6 mm). The calculated results of the electric potential distribution in the F-TENG are shown in Figure 2b. It has the largest electrical potential with up to about 150 V when the PTFE balls approach the top Cu foil (i) or bottom Cu foil (ii) electrode. The electric potential is found to decrease dramatically when the PTFE balls occur at the middle position between the two Cu foil (i and ii) electrodes. The calculated results of the electric potential distribution in the CSS-TENG under the different positions are depicted in Figure 2c. When the two surfaces of the FEP film and Cu foil (vi) are overlapped and contact each other exactly, the calculated electrical potential difference between the two electrodes is zero V (Figure 2cI). Then, with the sliding of Cu foil (vi) relative to the FEP film, the electric potential on the FEP film was found to gradually increase (Figure 2cII); when Cu foil (vi) approached the edge of the FEP film, it has the largest electrical potential, up to about 400 V (Figure 2cIII). The electric potential on Cu foil (vi) was found to decrease dramatically when leaving and approaching the FEP film, as depicted in Figure 3b (Figure 2cVI). Based on the converting process, a potential is generated to keep the charge balance according to the simulation, and the generated current can be essentially described by the second terms (polarization charge) of the corresponding displacement current in Maxwell's equation, as proposed by Wang. In a nutshell, the transition process presented in Figure 2b,c is referred to as the Wang transition.

2.3. Electrical Output Performances of the TV-TENG.

To characterize the output performance of the CSS-TENG with different triboelectric materials (FEP, PTFE, PI, PA11, and PET film), we fabricated the CSS-TENG with a contact area of 40 × 60 mm under the same wind speed of 2 m/s, and the results are shown in Figure 3a−c. The output performances of the open-circuit voltage (V_{OC}), short-circuit current (I_{SC}), and transferred charges (ΔQ_{SC}) of the device are the greatest from the FEP film material, which are 136.34 V, 28.75 μA, and 72.97 nC, respectively, and its surface charge density can be calculated as 30.4 μC m^{-2}. The reason is that the F element in the FEP material is higher and it is easier to obtain electrons. Moreover, in order to study the influence of different triboelectric materials on the output performance of the F-TENG, the Cu electrode was not changed and different counter triboelectric materials (Cu, FEP, PTFE, PET, and PI film) were interacted with PTFE balls. The output performances of the F-TENG were studied under the same wind speed of 2 m/s and with each acrylic space filled with 16 PTFE balls, and the results are shown in Figure 3d−f. From the

https://doi.org/10.1021/acsami.1c16680
ACS Appl. Mater. Interfaces XXXX, XXX, XXX−XXX

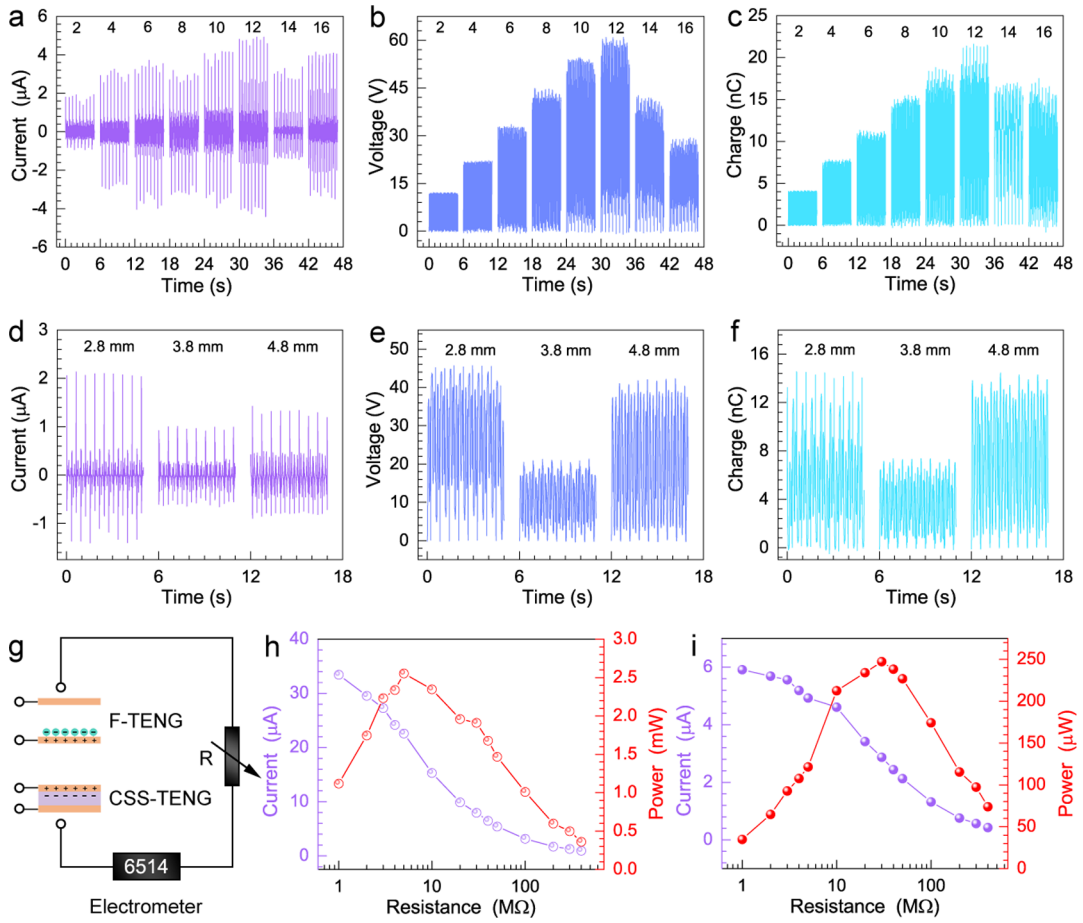

Figure 4. Electrical output performances of F-TENGs with different numbers of PTFE balls and different thicknesses of the acrylic plate. (a–c) Short-circuit current, open-circuit voltage, and transferred charge of the F-TENG with different numbers of PTFE balls. (d–f) Short-circuit current, open-circuit voltage, and transferred charge of the F-TENG with different thicknesses of the acrylic plate. (g) Schematic diagram of the peak power measurement system. (h,i) Peak current and peak power of the CSS-TENG and F-TENG.

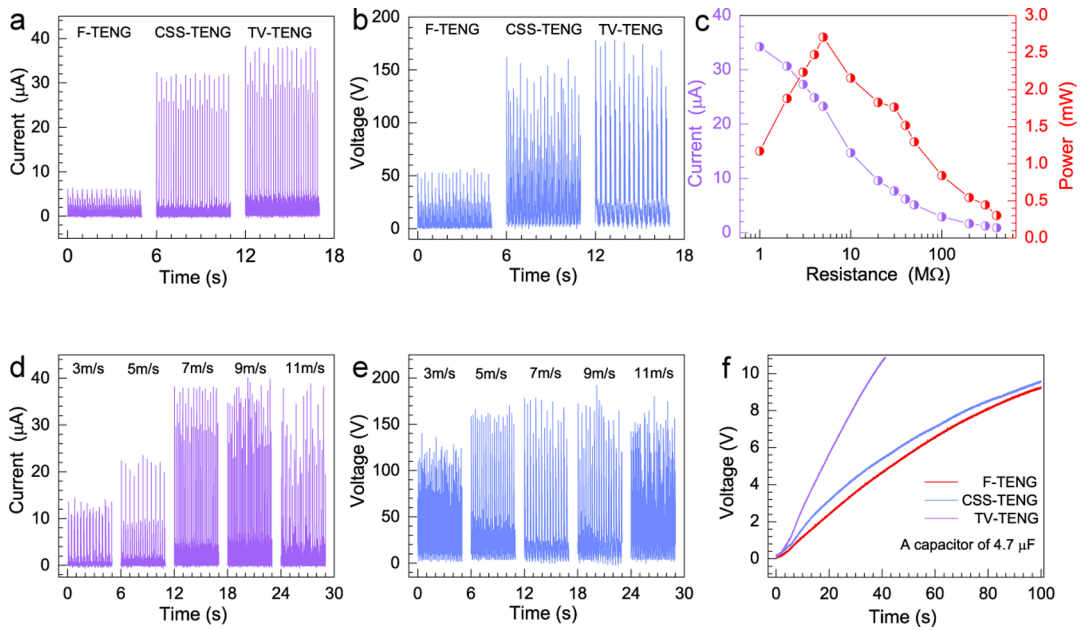

Figure 5. Electrical output performances of the F-TENG, C-TENG, and integrated TV-TENG under a wind speed of 7 m/s. (a,b) Short-circuit current and open-circuit voltage of the F-TENG, C-TENG, and integrated TV-TENG. (c) Peak current and peak power of the TV-TENG at a wind speed of 7 m/s. (d,e) Short-circuit current and open-circuit voltage of the integrated TV-TENG with different wind speeds. (f) Charging performance of the integrated TV-TENG under a capacitor of 4.7 μF.

https://doi.org/10.1021/acsami.1c16680
ACS Appl. Mater. Interfaces XXXX, XXX, XXX–XXX

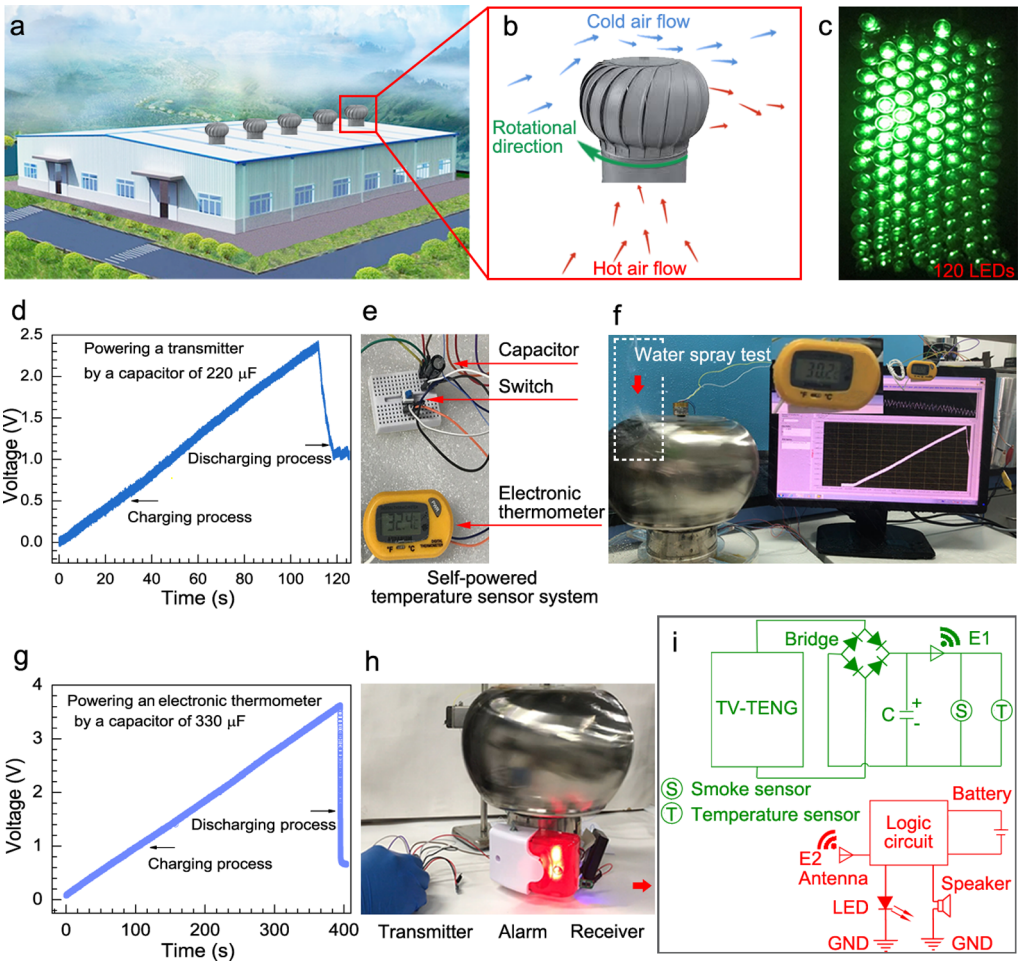

Figure 6. Application demonstrations of the TV-TENG harvesting irregular wind energy and as a self-powered environmental sensor system. (a) Schematic diagram showing the application scenarios of the TV-TENG in the smart factory field. (b) Basic working process of the TV-TENG caused by hot air rising. (c) Photograph of 120 commercial LEDs directly powered by the TV-TENG. (d) Charging and discharging process of a capacitor of 220 μF to power the thermometer under a wind speed of 7 m/s. (e) Photograph of the self-powered temperature sensor system. (f) Photograph of the working process of the self-powered temperature sensor system. (g) Charging and discharging process of a capacitor of 3300 μF to power a wireless transmitter under a wind speed of 7 m/s. (h) Photograph of the working process of the self-powered wireless early warning system. (i) Circuit diagrams and design of the self-powered system.

comparison, we know that the output V_{oc}, I_{sc}, and ΔQ_{SC} of the F-TENG revealed optimal results under the Cu triboelectric layer, which are 50.84 V, 4.1 μA, and 16.96 nC, respectively, and its surface charge density can be calculated as 7.07 μC m^{-2}. The reason is that the difference in electronegativity between the F element of the PTFE and the Cu element is farther, so the transferred charges are more.

In addition, the influence of PTFE balls of different numbers on the output performances of the F-TENG was studied, as shown in Figure 4a–c (Figure S1). Obviously, the output performances of the F-TENG increased and then decreased with increasing number of PTFE balls (2, 4, 6, 8, 10, 12, 14, and 16 balls). When the number of PTFE balls increased from 2 to 12, V_{oc} increased 5 times from 12 to 60 V, the I_{sc} increased 2.5 times from 1.8 to 4.7 μA, and the ΔQ_{SC} of the F-TENG increased 6.05 times from 3.8 to 23 nC. According to research findings, for the output V_{oc}, I_{sc}, and ΔQ_{SC} of the F-TENG revealed for ball numbers of 2, 4, 6, 8, 10, 12, 14, and 16, the optimal results were obtained for the PTFE ball number of 12, which are 60 V, 4.7 μA, and 23 nC, respectively, and its surface charge density can be calculated as 9.58 μC m^{-2}. The output performance of the F-TENG begins to decrease when the number of PTFE balls exceeds 12. The possible reason is that the space becomes overcrowded with increasing number of balls, resulting in restricted movement of the PTFE balls. We also studied the influence of the different movement distances of the PTFE balls (the thickness of the acrylic plate) on the output performance of the F-TENG, as shown in Figure 4d–f. The results found that the output performances of the F-TENG were the best when the thickness of the acrylic plate was 2.8 mm. Obviously, the V_{oc}, I_{sc}, and ΔQ_{SC} of the F-TENG reached 45.7 V, 2.1 μA, and 14.48 nC, respectively. The test method of instantaneous power of the TENGs is shown in Figure 4g. The instantaneous power of the CSS-TENG and the F-TENG is maximized at a load resistance 5 MΩ and 30 MΩ under a wind speed of 7 m/s, which corresponds to a peak power of 2.55 mW and 247 μW, as can be seen in Figure 4h–,i, respectively.

Furthermore, we studied the influence of different wind speeds on the output performance of the TV-TENG device, which is composed of the F-TENG and the CSS-TENG integrated together on a turbine vent with a volume of about 0.0064 m^3. Then, a comparison of the output performance is conducted for the F-TENG, CSS-TENG, and TV-TENG

https://doi.org/10.1021/acsami.1c16680
ACS Appl. Mater. Interfaces XXXX, XXX, XXX–XXX

under the same wind speed condition of 7 m/s, as shown in Figure 5a,b. Obviously, the I_{sc} and V_{oc} of the TV-TENG reached 38.2 μA and 178.2 V, respectively, and the accumulated contribution of the CSS-TENG on the I_{sc} and V_{oc} was more than 80%. The instantaneous power of the TV-TENG is maximized, which corresponds to a peak power of 2.71 mW at a load resistance 5 MΩ, as can be seen in Figure 5c. Considering the most suitable range of wind speeds, the output performance of TV-TENG was tested at different wind speeds, as shown in Figure 5d,e. On increasing the wind speed from 3 to 7 m/s, the values of I_{sc} and V_{oc} both increased gradually, which then tends to saturate with increasing wind speeds. The charging performance the F-TENG, CSS-TENG, and TV-TENG for different capacitors is investigated under the same wind speed condition of 7 m/s, as shown in Figure 5f. A capacitor of 4.7 μF was charged from 0 to 11 V within 40 s by the TV-TENG, and the charging times of the capacitor were 100, 85, and 35 s using the F-TENG, CSS-TENG, and TV-TENG, respectively, when the charging voltage of the capacitor was raised to the same value of 9.3 V. The experimental results show that the device exhibits good performance for harvesting wind energy. The TV-TENG exhibits a good mechanical stability as shown in Figure S4. It can continuously work for more than 40,000 cycles without an obvious decrease.

2.4. Self-Powered On-Site Industrial Monitoring System. Figure 6a depicts prospective applications of the TV-TENG by harvesting environmental irregular wind energy to provide a distributed power source for low-power sensors and other micro-electronic devices in industrial production, and the basic working process of the TV-TENG caused by hot air rising is shown in Figure 6b. The experimental results show that the device exhibits good performance for harvesting wind energy, lighting up 120 serially connected commercial LEDs directly, as shown in Figure 6c. The self-powered temperature sensor system was developed for measuring ambient temperature in an industrial environment, which includes a TV-TENG, a matched capacitor and electronic thermometer, and so forth, and its core is the TV-TENG as a sustainable power source by harvesting wind energy. Figure 6d shows the charging and discharging curve of a capacitor of 220 μF to power the thermometer under a wind speed of 7 m/s. After the capacitor was charged to 2.4 V in 110 s, the thermometer was connected to the circuit and turned on to measure the water temperature, as shown in supplementary Video S1 (Supporting Information). The photographs of the system and working process are shown in Figure 6e,f. Meanwhile, the system has good waterproofing and sealing function that can be used in the rain, meeting the requirements of various industries and outdoor working, as shown in supplementary Videos S2 and S3 (Figures S2 and S3 in the Supporting Information). To demonstrate its waterproofness and applicability, the above-mentioned results were obtained under the conditions of water drenching. The results confirm that the TV-TENG has excellent waterproofness and stability and can be used in the rain for a long time without affecting the electric performance of the system, which can be verified by the slopes of the charging curves showing no change. Then, a self-powered wireless early warning system was designed and successfully tested for monitoring production safety, which is composed of a TV-TENG, a set of a wireless transmitter and receiver, and a capacitor of 330 μF. Figure 6g shows the charging and discharging curve of the capacitor of 330 μF to power a wireless transmitter under a wind speed of 7 m/s. The wireless transmitter can send signals to the receiver at a long distance of above 10 m, and we only show the case when they are placed together due to the laboratory space limitation. After the capacitor of 330 μF was charged from 0 to about 3.62 V in 394 s, the transmitter was powered up to send a signal to the receiver when the switch was closed, which will trigger the alarm to send out sound and light. The photograph of the working process is shown in Figure 6h and supplementary Video S4. The circuit diagrams and design of the self-powered system are shown in Figure 6i, which responds in time to trigger the buzzer to emit a buzzing alarm. In the practical application process, the charging voltage of the capacitor reached a matching operating voltage in a shorter period of time outdoors in a windy environment, where the system started and entered the real-time monitoring state. It was predictable that the warning time shortened with the increase in wind speed, which implies that the TV-TENG can be used to forecast the temperature changes and provide pre-warning on production safety.

3. CONCLUSIONS

In summary, we have presented a practical TV-TENG device, which can be utilized as both an irregular wind harvester and a sustainable power source that is especially suitable to integrating a self-powered sensing system on the rooftops of buildings. The TV-TENG is composed of two F-TENGs and two CSS-TENGs and integrated together on a turbine vent with a volume of about 0.0064 m^3. It efficiently achieved sliding/vibration energy harvesting caused by the irregular wind from between adjacent buildings relying on the unique structural design and the characteristics of irregular wind. The TV-TENG generates an open-circuit voltage of up to 178.2 V, a short-circuit current of 38.2 μA, and a corresponding peak power of 2.71 mW under an external load of 5 MΩ, which can be used to directly light up 120 commercial LEDs. Furthermore, relying on the TV-TENG as a sustainable power source, self-powered temperature sensing and wireless early warning systems have been developed, which improved easiness and simpleness of industrial production safety monitoring. It is a novel approach for harvesting irregular wind energy and is sensitive, reliable, and easy to use, while having the advantages of waterproofness and ventilation. This work greatly expands the applicability of TENGs as energy harvesters for irregular wind and self-powered sensing systems, and it can be widely used for environmental monitoring and in the chemical industry and many other fields.

4. EXPERIMENTAL SECTION

Fabrication of the F-TENG device: First, a laser cutting machine was used to cut 16 rectangular cavities array (width of 34 mm and thickness of 2.5 mm) in the center of an acrylic plate (length of 60 mm, width of 40 mm, and thickness of 2.8 mm), and its back was sealed to the same side of Cu whose back was pasted with PET (thickness of 0.125 mm). Subsequently, a certain amount of PTFE balls was incorporated into each cuboid cavity, with the diameter of the ball being 2.1 mm, using the same area of Cu whose back was pasted with wider and thicker PET (width of 55 mm and thickness of 0.25 mm) to seal the front of the acrylic sheet, and the extended PET was fixed on the shaft of the turbine vent as a vibrating arm.

The production of the CSC-TENG device: Sponge glue with the same size as the acrylic plate was pasted on the back of the wider and thicker PET in the F-TENG. Then, a Cu film of the same size was pasted on the sponge glue as the electrode. Subsequently, the FEP film (80 μm) was pasted on the Cu film as the friction layer of the

https://doi.org/10.1021/acsami.1c16680
ACS Appl. Mater. Interfaces XXXX, XXX, XXX−XXX

negative electrode; the other electrode was pasted on PET (length of 60 mm, width of 55 mm, and thickness of 0.2 mm) with the same size of the Cu film as the positive electrode of the CSS-TENG, and it was fixed on the curved blades of the turbine vent. Two sets of F-TENGs and CSC-TENGs were installed in the turbine vent to form the TV-TENG. The output performance of TV-TENG was measured using a current preamplifier (Keithley 6514 electrometer), while the output voltage of TV-TENG devices at wind speeds of nearly 7 m/s was measured using a digital oscilloscope (Agilent InfiniiVision 2000X).

■ ASSOCIATED CONTENT

Supporting Information

The Supporting Information is available free of charge at https://pubs.acs.org/doi/10.1021/acsami.1c16680.

Detailed fabrication process of the TV-TENG; electrical output performances of the F-TENG under one triggering; screenshots of the charging process of the 220 μF capacitor under the conditions of continuous water drenching; screenshots of slope change of charging curves before and after water drenching; and mechanical stability of the TV-TENG (PDF)

Powering the thermometer to measure the water temperature (AVI)

Exhibiting the good waterproofness of the system (AVI)

Exhibiting the good sealing function of the system (AVI)

Powering the alarm (AVI)

■ AUTHOR INFORMATION

Corresponding Authors

Baodong Chen − *Beijing Institute of Nanoenergy and Nanosystems, Chinese Academy of Sciences, Beijing 101400, P. R. China; School of Nanoscience and Technology, University of Chinese Academy of Sciences, Beijing 100049, P. R. China; Institute of Applied Nanotechnology, Jiaxing, Zhejiang 314031, P. R. China;* orcid.org/0000-0002-4647-0089; Email: chenbaodong@binn.cas.cn

Zhong Lin Wang − *Beijing Institute of Nanoenergy and Nanosystems, Chinese Academy of Sciences, Beijing 101400, P. R. China; School of Nanoscience and Technology, University of Chinese Academy of Sciences, Beijing 100049, P. R. China; School of Materials Science and Engineering, Georgia Institute of Technology, Atlanta, Georgia 30332-0245, United States;* orcid.org/0000-0002-5530-0380; Email: zlwang@gatech.edu

Authors

Jianjun Zhang − *Beijing Institute of Nanoenergy and Nanosystems, Chinese Academy of Sciences, Beijing 101400, P. R. China; College of Chemistry and Chemical Engineering, Center on Nanoenergy Research, Guangxi University, Nanning 530004, P. R. China*

Yanshuo Sun − *Beijing Institute of Nanoenergy and Nanosystems, Chinese Academy of Sciences, Beijing 101400, P. R. China; College of Chemistry and Chemical Engineering, Center on Nanoenergy Research, Guangxi University, Nanning 530004, P. R. China*

Jin Yang − *Beijing Institute of Nanoenergy and Nanosystems, Chinese Academy of Sciences, Beijing 101400, P. R. China; College of Chemistry and Chemical Engineering, Center on Nanoenergy Research, Guangxi University, Nanning 530004, P. R. China*

Tao Jiang − *Beijing Institute of Nanoenergy and Nanosystems, Chinese Academy of Sciences, Beijing 101400, P. R. China; School of Nanoscience and Technology, University of Chinese Academy of Sciences, Beijing 100049, P. R. China*

Wei Tang − *Beijing Institute of Nanoenergy and Nanosystems, Chinese Academy of Sciences, Beijing 101400, P. R. China; School of Nanoscience and Technology, University of Chinese Academy of Sciences, Beijing 100049, P. R. China*

Complete contact information is available at: https://pubs.acs.org/10.1021/acsami.1c16680

Author Contributions

J.Z. and Y.S. contributed equally to this work. B.C. and Z.L.W. proposed and supervised the project. J.Z. participated in all aspects of this work from device fabrication to characterization and data processing. W.T. designed the structures of the TV-TENG. T.J. and Y.S. were involved in device fabrication. J.Y. participated in capturing videos of equipment applications. All authors discussed the results and commented on the article.

Notes

The authors declare no competing financial interest.

■ ACKNOWLEDGMENTS

J.Z. and Y. S. contributed equally to this work. This work was supported by the Beijing Natural Science Foundation (grant no. 2192062), the National Natural Science Foundation of China (grant no. 51502147, 51702018 and 11704032), the National Key R & D Project from Minister of Science and Technology (2016YFA0202704), and the Beijing Municipal Science and Technology Commission (Z181100003818016 and Y3993113DF).

■ REFERENCES

(1) Chen, B. D.; Tang, W.; He, C.; Deng, C. R.; Yang, L. J.; Zhu, L. P.; Chen, J.; Shao, J. J.; Liu, L.; Wang, Z. L. Water Wave Energy Harvesting and Self-Powered Liquid-Surface Fluctuation Sensing Based on Bionic-Jellyfish Triboelectric Nanogenerator. *Mater. Today* **2018**, *21*, 88−97.

(2) Tang, W.; Jiang, T.; Fan, F. R.; Yu, A. F.; Zhang, C.; Cao, X.; Wang, Z. L. Liquid-Metal Electrode for High-Performance Triboelectric Nanogenerator at an Instantaneous Energy Conversion Efficiency of 70.6%. *Adv. Funct. Mater.* **2015**, *25*, 3718−3725.

(3) Liu, S.; Li, X.; Wang, Y.; Yang, Y.; Meng, L.; Cheng, T.; Wang, Z. L. Magnetic Switch Structured Triboelectric Nanogenerator for Continuous and Regular Harvesting of Wind Energy. *Nano Energy* **2021**, *83*, 105851.

(4) Qian, J.; Jing, X. Wind-Driven Hybridized Triboelectric-Electromagnetic Nanogenerator and Solar Cell as a Sustainable Power Unit for Self-Powered Natural Disaster Monitoring Sensor Networks. *Nano Energy* **2018**, *52*, 78−87.

(5) Chen, J.; Yang, J.; Guo, H.; Li, Z.; Zheng, L.; Su, Y.; Wen, Z.; Fan, X.; Wang, Z. L. Automatic Mode Transition Enabled Robust Triboelectric Nanogenerators. *ACS Nano* **2015**, *9*, 12334−12343.

(6) Zhang, L.; Zhang, B.; Chen, J.; Jin, L.; Deng, W.; Tang, J.; Zhang, H.; Pan, H.; Zhu, M.; Yang, W.; Wang, Z. L. Lawn Structured Triboelectric Nanogenerators for Scavenging Sweeping Wind Energy on Rooftops. *Adv. Mater.* **2016**, *28*, 1650−1656.

(7) Zhu, G.; Chen, J.; Zhang, T.; Jing, Q.; Wang, Z. L. Radial-Arrayed Rotary Electrification for High Performance Triboelectric Generator. *Nat. Commun.* **2014**, *5*, 3426.

(8) Zhang, B.; Chen, J.; Jin, L.; Deng, W.; Zhang, L.; Zhang, H.; Zhu, M.; Yang, W.; Wang, Z. L. Rotating-Disk-Based Hybridized Electromagnetic-Triboelectric Nanogenerator for Sustainably Powering Wireless Traffic Volume Sensors. *ACS Nano* **2016**, *10*, 6241−6247.

(9) Yang, Y.; Zhu, G.; Zhang, H.; Chen, J.; Zhong, X.; Lin, Z.-H.; Su, Y.; Bai, P.; Wen, X.; Wang, Z. L. Triboelectric Nanogenerator for

Harvesting Wind Energy and as Self-Powered Wind Vector Sensor System. *ACS Nano* **2013**, *7*, 9461−9468.
(10) Xie, Y.; Wang, S.; Lin, L.; Jing, Q.; Lin, Z.-H.; Niu, S.; Wu, Z.; Wang, Z. L. Rotary Triboelectric Nanogenerator Based on a Hybridized Mechanism for Harvesting Wind Energy. *ACS Nano* **2013**, *7*, 7119−7125.
(11) Blaabjerg, F.; Ma, K. K. Future on Power Electronics for Wind Turbine Systems. *J. Emerg. Sel. Top. Power Syst.* **2013**, *1*, 139−152.
(12) Fu, X.; Xu, S.; Gao, Y.; Zhang, X.; Liu, G.; Zhou, H.; Lv, Y.; Zhang, C.; Wang, Z. L. Breeze-Wind-Energy-Powered Autonomous Wireless Anemometer Based on Rolling Contact-Electrification. *ACS Energy Lett.* **2021**, *6*, 2343−2350.
(13) Ren, Z.; Wang, Z.; Liu, Z.; Wang, L.; Guo, H.; Li, L.; Li, S.; Chen, X.; Tang, W.; Wang, Z. L. Energy Harvesting from Breeze Wind (0.7−6 m s−1) Using Ultra-Stretchable Triboelectric Nanogenerator. *Adv. Energy Mater.* **2020**, *10*, 2001770.
(14) Zhao, Z.; Pu, X.; Du, C.; Li, L.; Jiang, C.; Hu, W.; Wang, Z. L. Freestanding Flag-Type Triboelectric Nanogenerator for Harvesting High-Altitude Wind Energy from Arbitrary Directions. *ACS Nano* **2016**, *10*, 1780−1787.
(15) Ravichandran, A. N.; Calmes, C.; Serres, J. R.; Ramuz, M.; Blayac, S. Compact and High Performance Wind Actuated Venturi Triboelectric Energy Harvester. *Nano Energy* **2019**, *62*, 449−457.
(16) Yong, S.; Wang, J.; Yang, L.; Wang, H.; Luo, H.; Liao, R.; Wang, Z. L. Auto-Switching Self-Powered System for Efficient Broad-Band Wind Energy Harvesting Based on Dual-Rotation Shaft Triboelectric Nanogenerator. *Adv. Energy Mater.* **2021**, *11*, 2101194.
(17) Fan, F.-R.; Tian, Z.-Q.; Wang, Z. L. Flexible Triboelectric Generator. *Nano Energy* **2012**, *1*, 328−334.
(18) Jiang, T.; Pang, H.; An, J.; Lu, P.; Feng, Y.; Liang, X.; Zhong, W.; Wang, Z. L. Robust Swing-Structured Triboelectric Nanogenerator for Efficient Blue Energy Harvesting. *Adv. Energy Mater.* **2020**, *10*, 2000064.
(19) Chen, P.; An, J.; Shu, S.; Cheng, R.; Nie, J.; Jiang, T.; Wang, Z. L. Super-Durable, Low-Wear, and High-Performance Fur-Brush Triboelectric Nanogenerator for Wind and Water Energy Harvesting for Smart Agriculture. *Adv. Energy Mater.* **2021**, *11*, 2003066.
(20) Zhang, J.; Zheng, Y.; Xu, L.; Wang, D. Oleic-Acid Enhanced Triboelectric Nanogenerator with High Output Performance and Wear Resistance. *Nano Energy* **2020**, *69*, 104435.
(21) Zhang, L.; Zhang, B.; Chen, J.; Jin, L.; Deng, W.; Tang, J.; Zhang, H.; Pan, H.; Zhu, M.; Yang, W.; Wang, Z. L. Lawn Structured Triboelectric Nanogenerators for Scavenging Sweeping Wind Energy on Rooftops. *Adv. Mater.* **2016**, *28*, 1650−1656.
(22) Wen, X.; Yang, W.; Jing, Q.; Wang, Z. L. Harvesting Broadband Kinetic Impact Energy from Mechanical Triggering/Vibration and Water Waves. *ACS Nano* **2014**, *8*, 7405−7412.
(23) Xiao, X.; Zhang, X.; Wang, S.; Ouyang, H.; Chen, P.; Song, L.; Yuan, H.; Ji, Y.; Wang, P.; Li, Z.; Xu, M.; Wang, Z. L. Honeycomb Structure Inspired Triboelectric Nanogenerator for Highly Effective Vibration Energy Harvesting and Self-Powered Engine Condition Monitoring. *Adv. Energy Mater.* **2019**, *9*, 1902460.
(24) Yang, X.; Xu, L.; Lin, P.; Zhong, W.; Bai, Y.; Luo, J.; Chen, J.; Wang, Z. L. Macroscopic Self-Assembly Network of Encapsulated High-Performance Triboelectric Nanogenerators for Water Wave Energy Harvesting. *Nano Energy* **2019**, *60*, 404−412.
(25) Zhang, B.; Zhang, L.; Deng, W.; Jin, L.; Chun, F.; Pan, H.; Gu, B.; Zhang, H.; Lv, Z.; Yang, W.; Wang, Z. L. Self-Powered Acceleration Sensor Based on Liquid Metal Triboelectric Nanogenerator for Vibration Monitoring. *ACS Nano* **2017**, *11*, 7440−7446.
(26) Zhao, C.; Zhang, Q.; Zhang, W.; Du, X.; Zhang, Y.; Gong, S.; Ren, K.; Sun, Q.; Wang, Z. L. Hybrid Piezo/Triboelectric Nanogenerator for Highly Efficient and Stable Rotation Energy Harvesting. *Nano Energy* **2019**, *57*, 440−449.
(27) Tang, W.; Zhang, C.; Han, C. B.; Wang, Z. L. Enhancing Output Power of Cylindrical Triboelectric Nanogenerators by Segmentation Design and Multilayer Integration. *Adv. Funct. Mater.* **2014**, *24*, 6684−6690.
(28) Tang, Q.; Yeh, M.-H.; Liu, G.; Li, S.; Chen, J.; Bai, Y.; Feng, L.; Lai, M.; Ho, K.-C.; Guo, H.; Hu, C. Whirligig-Inspired Triboelectric Nanogenerator with Ultrahigh Specific Output as Reliable Portable Instant Power Supply for Personal Health Monitoring Devices. *Nano Energy* **2018**, *47*, 74−80.
(29) Chen, P.; An, J.; Cheng, R.; Shu, S.; Berbille, A.; Jiang, T.; Wang, Z. L. Rationally Segmented Triboelectric Nanogenerator with a Constant Direct-Current Output and Low Crest Factor. *Energy Environ. Sci.* **2021**, *14*, 4523−4532.
(30) Wu, Z.; Guo, H.; Ding, W.; Wang, Y. C.; Zhang, L.; Wang, Z. L. A Hybridized Triboelectric-Electromagnetic Water Wave Energy Harvester Based on a Magnetic Sphere. *ACS Nano* **2019**, *13*, 2349−2356.
(31) Wang, J.; Wu, Z.; Pan, L.; Gao, R.; Zhang, B.; Yang, L.; Guo, H.; Liao, R.; Wang, Z. L. Direct-Current Rotary-Tubular Triboelectric Nanogenerators Based on Liquid-Dielectrics Contact for Sustainable Energy Harvesting and Chemical Composition Analysis. *ACS Nano* **2019**, *13*, 2587−2598.
(32) Li, X.; Tao, J.; Wang, X.; Zhu, J.; Pan, C.; Wang, Z. L. Networks of High Performance Triboelectric Nanogenerators Based on Liquid-Solid Interface Contact Electrification for Harvesting Low-Frequency Blue Energy. *Adv. Energy Mater.* **2018**, *8*, 1800705.
(33) Kim, D.; Tcho, I.-W.; Choi, Y.-K. Triboelectric Nanogenerator Based on Rolling Motion of Beads for Harvesting Wind Energy as Active Wind Speed Sensor. *Nano Energy* **2018**, *52*, 256−263.
(34) Xi, Y.; Guo, H.; Zi, Y.; Li, X.; Wang, J.; Deng, J.; Li, S.; Hu, C.; Cao, X.; Wang, Z. L. Multifunctional TENG for Blue Energy Scavenging and Self-Powered Wind-Speed Sensor. *Adv. Energy Mater.* **2017**, *7*, 1602397.
(35) Wen, J.; Chen, B.; Tang, W.; Jiang, T.; Zhu, L.; Xu, L.; Chen, J.; Shao, J.; Han, K.; Ma, W.; Wang, Z. L. Harsh-Environmental-Resistant Triboelectric Nanogenerator and Its Applications in Autodrive Safety Warning. *Adv. Energy Mater.* **2018**, *8*, 1801898.
(36) Wang, Z.; An, J.; Nie, J.; Luo, J.; Shao, J.; Jiang, T.; Chen, B.; Tang, W.; Wang, Z. L. A Self-Powered Angle Sensor at Nanoradian-Resolution for Robotic Arms and Personalized Medicare. *Adv. Mater.* **2020**, *32*, No. e2001466.
(37) An, J.; Wang, Z.; Jiang, T.; Chen, P.; Liang, X.; Shao, J.; Nie, J.; Xu, M.; Wang, Z. L. Reliable Mechatronic Indicator for Self-Powered Liquid Sensing Toward Smart Manufacture and Safe Transportation. *Mater. Today* **2020**, *41*, 10−20.
(38) Seol, M.-L.; Woo, J.-H.; Jeon, S.-B.; Kim, D.; Park, S.-J.; Hur, J.; Choi, Y.-K. Vertically Stacked Thin Triboelectric Nanogenerator for Wind Energy Harvesting. *Nano Energy* **2015**, *14*, 201−208.
(39) Wright, A. K.; Wood, D. H. The Starting and Low Wind Speed Behaviour of a Small Horizontal Axis Wind Turbine. *J. Wind Eng. Ind. Aerod.* **2004**, *92*, 1265−1279.
(40) Petroni, S.; Rizzi, F.; Guido, F.; Cannavale, A.; Donateo, T.; Ingrosso, F.; Mastronardi, V. M.; Cingolani, R.; De Vittorio, M. Flexible AlN Flags for Efficient Wind Energy Harvesting at Ultralow Cut-In Wind Speed. *RSC Adv.* **2015**, *5*, 14047−14052.
(41) Xi, Y.; Wang, J.; Zi, Y.; Li, X.; Han, C.; Cao, X.; Hu, C.; Wang, Z. High Efficient Harvesting of Underwater Ultrasonic Wave Energy by Triboelectric Nanogenerator. *Nano Energy* **2017**, *38*, 101−108.
(42) Zou, H.; Zhang, Y.; Guo, L.; Wang, P.; He, X.; Dai, G.; Zheng, H.; Chen, C.; Wang, A. C.; Xu, C.; Wang, Z. L. Quantifying the Triboelectric Series. *Nat. Commun.* **2019**, *10*, 1427.
(43) Shao, J.; Willatzen, M.; Wang, Z. L. Theoretical Modeling of Triboelectric Nanogenerators (TENGs). *J. Appl. Phys.* **2020**, *128*, 111101.
(44) Shao, J.; Willatzen, M.; Jiang, T.; Tang, W.; Chen, X.; Wang, J.; Wang, Z. L. Quantifying the Power Output and Structural Figure-of-Merits of Triboelectric Nanogenerators in a Charging System Starting from the Maxwell's Displacement Current. *Nano Energy* **2019**, *59*, 380−389.

https://doi.org/10.1021/acsami.1c16680
ACS Appl. Mater. Interfaces XXXX, XXX, XXX−XXX